CHEMISTRY OF MATERIALS

pubs.acs.org/cm

Article

pH-Responsive Gelation in Metallo-Supramolecular Polymers Based on the Protic Pyridinedicarboxamide Ligand

Mostafa Ahmadi,* Farhad Panahi, Naeimeh Bahri-Laleh, Mohammad Sabzi, Gerard Pareras, Bruno N. Falcone, and Albert Poater*

Cite This: *Chem. Mater.* 2022, 34, 6155−6169

Read Online

ACCESS | Metrics & More | Article Recommendations | Supporting Information

ABSTRACT: Pyridinedicarboxamide (PDCA) ligands have been widely integrated into different polymer chemistries and provided promising self-healing properties in bulk upon adding specific metal ions. However, their application in the development of synthetic hydrogels is limited due to the lack of clear kinetics and thermodynamic data. To fill this gap, we study the dynamics of polymer hydrogels formed by the condensation of linear poly(ethylene glycol) (PEG) precursors and the PDCA ligand, followed by the complexation with different metal ions at various pH values. Rheological studies reveal an unprecedented ability of PDCA in complexation with $Co^{2+/3+}$ and Ni^{2+} at elevated pH values, but in contrast with former reports, not with Fe^{3+} and Zn^{2+}. Moreover, $Co^{2+/3+}$ gels demonstrate lower equilibrium constants resulting in faster and more efficient self-healing compared to those made by Ni^{2+}. Spectroscopic UV and Fourier transform infrared (FTIR) studies also suggest structural modifications in the presence of the gel-forming metal ions but not the others. To explain these results, we employ static and periodic density functional theory (DFT) simulations. Static DFT indeed reveals that the binding interaction is clearly stronger for Co and Ni, and Fe shows the poorest values by far. The most stable complex geometry is octahedral, in which the central pyridyl, one lateral deprotonated amide, and one carbonyl participate in the metal coordination. Moreover, the periodic calculations unveil an overstabilization effect due to the noncovalent interactions between the PEG segments, which results in their torsion and formation of a helicoidal-like structure.

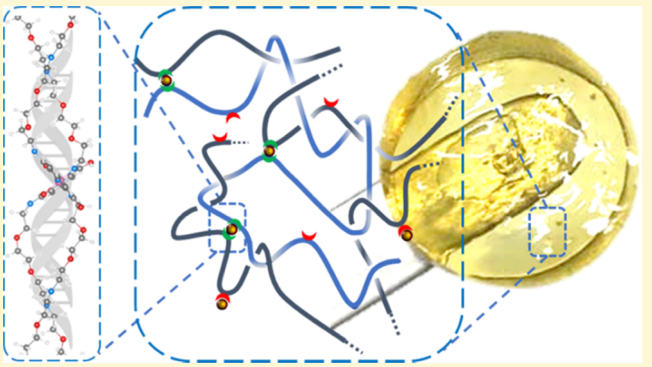

1. INTRODUCTION

Organic hydrogels are among the prevailing materials in nature, as they constitute the main body of most living creatures. Therefore, synthetic hydrogels are extensively used in biotechnology-related applications like tissue engineering and drug delivery.[1] To this end, imparting biomimetic functions like self-healing and stimuli-responsiveness is the key feature to developing novel polymeric hydrogels.[2−5] This is mainly accomplished by the introduction of reversible transient bonds within the microstructure of polymer chains, as the dynamics of their reversible dissociation can be tuned to meet the required stimuli-responsiveness and self-healing rates.[6−10] As such, correlating the microscopic characteristics of reversible bonds to the macroscopic properties of transient polymeric hydrogels is necessary for the customized development of hydrogels employed in specific bio-inspired applications.[11,12]

One of the enduring goals in the development of biomimetic synthetic materials is self-healing. Many natural hydrogels are strong and elastic, but they can perfectly cure internal damages in a reasonable time.[13] In contrast, there is a traditional trade-off between mechanical performance and self-healing ability in synthetic hydrogels.[14] One of the recent bio-inspired approaches to overcoming this dilemma is to combine two types of dynamics with significantly different characteristic times, so that the slow mode contributes to the high mechanical strength and the fast mode provides self-healing. This follows nature's widely observed trick of integrating different transient bonds in sophisticated hierarchical structures to function adaptively at various time and length scales.[15] A popular example of these natural materials is the sea mussel byssus thread, which consists of a soft core rich in histidine and a hard shell comprising catechol in a multiphase structure.[16−18] The coordination of the former ligand with divalent zinc ions that are selectively absorbed from seawater and the complexation of the latter with trivalent iron ions that are widely found on seashores provide the key combination of fast and slow

Received: May 3, 2022
Revised: June 8, 2022
Published: June 23, 2022

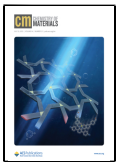

dynamics, which is required to provide simultaneously fast self-healing and high mechanical strength. Inspired by such elegant designs, Guan and co-workers have incorporated weak supramolecular bonds, based on metal−ligand coordination or hydrogen bonds, into the polyacrylate arms of a comb structure with a polystyrene backbone.[19,20] The microphase separation of the low glass-transition temperature (T_g) arm from the high-T_g backbone yields high mechanical strength originating from the dispersed hard phase and fast healing by the reversible dissociation of transient bonds within the soft phase.[21] This approach has recently been further expanded by employing orthogonal combinations of more defined transient bonds, even from different natures, but with significantly different lifetimes.[22−28]

Among all of the transient bonds used, metal−ligand complexes are widely employed for the development of biomimetic transient hydrogels, not only because they can be formed simply in water but since their strength and stability can be freely tuned over several orders of magnitude by a mere change of the metal ion, its oxidation state, and the selection from the extensive library of ligands.[29−32] As such, the necessary coexistence of two relaxation modes with significantly different lifetimes to achieve self-healing can be realized simply by employing two different metal ions or two various ligands.[27,28,33−35] In this regard, pyridinedicarboxamide (PDCA) is a unique tridentate ligand that is reported to form two distinct coordination bonds with significantly different dynamics upon complexation with the Fe^{3+} ion.[36−39] Therefore, it has been widely integrated into different polymer chemistries and has shown promising self-healing properties.[40,41] Despite the acceptable individual performance, it has also been utilized in combination with carboxylate-based ligands, which are also capable of complexation with the Fe^{3+} ion, and have shown synergistic properties.[38,41] The small-molecule variant of the PDCA ligand has shown a remarkable pH-sensitive complexation with covalent bond-like stability under basic conditions, which is a characteristic of protic ligands.[39] Nevertheless, there is no information on the kinetics, thermodynamics, and pH responsivity of PDCA complexes, which otherwise could be employed to expand their utility as novel building blocks for metallo-supramolecular polymer networks.

To fill this gap, herein we study the dynamics of model polymer networks formed by the condensation of linear poly(ethylene glycol) (PEG) precursor and PDCA ligand and the subsequent complexation with different metal ions at various pH values and oxidation states. We come up with unprecedented results that challenge the former reports on the ability of the PDCA ligand in complexation with Fe^{3+} and Zn^{2+} ions. Our rheological results are consistent with UV and FTIR spectroscopy studies. To further explain these experimental findings, we follow the thermodynamics of complexation by density functional theory (DFT) simulations. Static and periodic DFT calculations are performed here to unveil mechanistic insights, and characterization techniques are used to understand the strength of coordination between the metal ions and the ligand chains and how the ligands are placed. As such, we offer a new understanding and application potential for the metallo-supramolecular polymer networks based on the protic PDCA ligand.

2. EXPERIMENTAL SECTION

2.1. Synthesis. 2,6-Pyridinedicarbonyl dichloride (Cl-PDCA) is purchased from Alfa Aesar. All other chemicals are purchased from Sigma-Aldrich and used without further purification. All solvents used for reactions are extra dry and purchased from Acros. The synthesis of amine-functionalized PEG precursor, $PEGNH_2$10k, has been reported elsewhere.[42,43] As the condensation reaction between PEG and PDCA is air- and moisture-sensitive, the $PEGNH_2$10k precursor (M_w = 10 kg mol^{-1}, PDI = 1.03, 3 g, 0.3 mmol) is first melted at 70 °C, dried *in vacuo* for 1 h, cooled to 0 °C, and then dissolved in dry dichloromethane (DCM, 15 mL). Triethylamine (0.25 mL, 1.8 mmol) is added dropwise, and the reaction is mixed at 0 °C for 2 h. Subsequently, a solution of 2,6-pyridinedicarboxylic acid chloride (61.2 mg, 0.3 mmol) in DCM (5 mL) is added dropwise. The resulting mixture is stirred at 0 °C for another 2 h and then warmed to room temperature and stirred for 2 days. The reaction mixture is concentrated *in vacuo* and precipitated in cold diethyl ether. The precipitate is filtered and dried to obtain the product, PEG10kPDCA, as a white powder. ^{1}H NMR (Figure S1) (400 MHz, DMSO-d_6) δ = 9.43 (t, J = 6.0 Hz, 1H), 8.18 (q, J = 5.2 Hz, 1H), 4.02−2.96 (m, 1017H) ppm.

2.2. Characterization. UV−Vis spectroscopy is used to calculate the functionalization degree and also to study the complexation of PDCA and various metal ions. Wavelengths between 200 and 700 nm are scanned at a rate of 200 nm min^{-1} on a Cary 300 UV−Vis spectrophotometer (Agilent Technologies) at room temperature. Functionalization degree is determined based on a calibration curve obtained from the small-molecule Cl-PDCA ligand in the chloroform. For this purpose, a stock solution of Cl-PDCA in the chloroform at a concentration of 1 mM is prepared and the evolution of the absorbance at 270 nm is followed by the stepwise dilution of the stock solution down to a concentration of 0.003 mM. Despite differences in the absorption spectra of Cl-PDCA and PEG10kPDCA, they both show local maxima at this specific wavelength, which can be employed to provide a relative estimate of the functionalization degree, as shown in Figure S2. Moreover, to follow the complexation of PEG10kPDCA with various metal ions, an aqueous solution of the PEG10kPDCA is combined with an aqueous solution of transition-metal ions. After 1 h, the designated volume of sodium hydroxide (10 mM) solution is added to yield an overall complex concentration of 25 μM, and after 24 h, the absorption spectra are acquired.

Rheological measurements are performed on a stress-controlled Anton Paar Physica MCR 301 rheometer with a 25 mm parallel plate geometry. Samples with 200 μL volume are prepared by adding 10 μL of the metal ion solution to a 160 μL polymer solution (125 g L^{-1}) and increasing the pH after 1 h by adding a 30 mL sodium hydroxide solution. Samples are allowed to rest and homogenize for 24 h before rheological measurements. Parameters to be studied include the molar ratio of hydroxyl to PDCA ligand (OH/PDCA) and the PDCA ligand to metal ions (PDCA/M); therefore, stock solutions of metal ions and sodium hydroxides with various concentrations were used to reach the desired ratios. The standard Anton Paar solvent trap, which includes a solvent reservoir and a sealed chamber, was used to avoid solvent evaporation. Moreover, after loading the samples and fixing the gap, a few drops of silicone oil are used to seal the surrounding samples. Rheological measurements include a three-step equilibration period (Υ = 0.01, ω = 1 rad s^{-1}) at 40, 25, and 10 °C, followed by a series of frequency sweep (Υ = 0.01, ω = 100−0.01 rad s^{-1}) at 10, 20, 25, 30, and 40 °C, followed by a series of stress relaxation (Υ = 0.1, ω = 1 rad s^{-1}) at 40, 30, 25, 20, and 10 °C. A 5 min time-sweep segment was placed between each sequential measurement to restore the equilibrium structure at the desired temperature. Finally, self-healing efficiency was examined at 25 °C by sequentially destroying the network structure at very high deformation amplitudes (Υ = 10, ω = 1 rad s^{-1}) and subsequent network reformation in the linear viscoelastic regime (Υ = 0.01, ω = 1 rad s^{-1}).

2.3. Computational Methods. The Gaussian 16 package is applied for conducting molecular modeling simulations.[44] Geometry optimizations are performed using B3LYP, *i.e.*, the hybrid GGA

https://doi.org/10.1021/acs.chemmater.2c01346
Chem. Mater. 2022, 34, 6155−6169

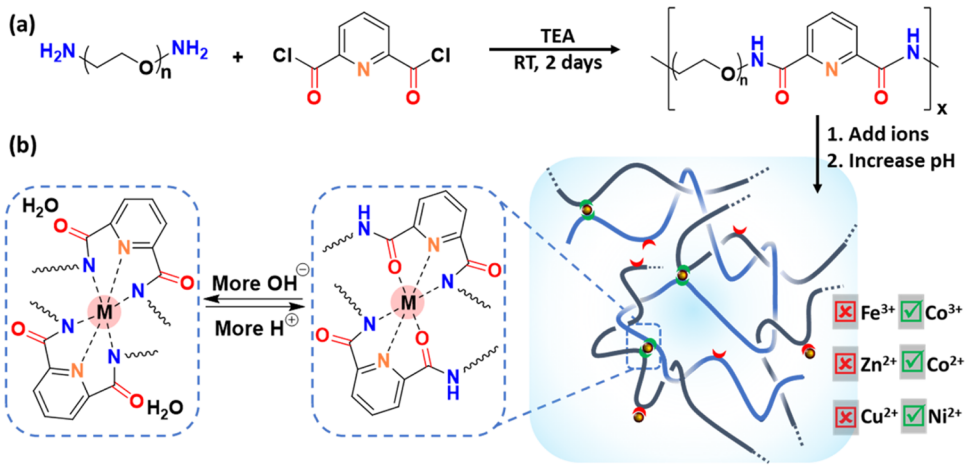

Figure 1. (a) Condensation reaction between $PEGNH_2$10k and Cl-PDCA. (b) Physical gels may form upon the addition of various metal ions and by increasing the pH. Progressive deprotonation occurs at higher pH values, which can result in the formation of bis-complexes with different coordination bonds.

functional of Becke, Lee, Parr, and Yang.[45−47] In the case of nonmetal atoms (*i.e.*, C, H, N, O, and Cl), the split-valence basis set (Def2SVP keyword in Gaussian)[48,49] is used, whereas for Fe, Co, Zn, and Ni, the small-core quasi-relativistic Stuttgart/Dresden effective core potential with an associated valence basis set (standard SDD keywords in Gaussian 16) is adopted.[50−52]

To approve the nature of the stationary points, frequency calculations are carried out. The reported free energies in this work include energies obtained at the B3LYP-D3/Def2TZVPP∼sdd//B3LYP-D3/Def2SVP level of theory corrected with zero-point energies, thermal corrections, and entropy effects evaluated at 298 K with the BP86/Def2SVP∼sdd method in the gas phase, omitting corrections of entropy and standard state of a 1 M concentration in solution.[53−55]

Even though the unit cell of ligands is excessively large and difficult to define for periodic DFT calculations, we perform the calculations on a fragment by CP2K to better understand how the ligands affect the metal centers in a network structure close to reality.

Calculations using the CP2K package[56] are performed at the density functional level of theory under periodic boundary conditions (PBE). The semilocal PBEsol functional is adopted,[57] using the DZVP-MOLOPT-SR-GTH Gaussian basis set for all of the atom types,[58] a cutoff of 500 Ry for the plane-wave auxiliary basis set, and SCF convergence set at 1.0×10^{-6}. The structures under study are constructed manually and fitted within a cubic box of $25 \times 25 \times 25$ $Å^3$, ensuring isolation in the *X* and *Z* directions and only periodicity on the *Y* axis, posteriorly performing cell optimizations to reduce lattice energy as well as relaxing the geometry and finally obtaining the optimized cell parameters (see Table S1).

Single-point calculations are then performed to calculate binding energies (BEs) between the organic part of the polymer and the relevant transition metal considering the basis set superimposition error (BSSE). Furthermore, the self-consistent continuum solvation (SCCS) model, as implemented in CP2K,[59] is also considered, employing dichloromethane and water as solvents. In CP2K, the interaction energy could be calculated by defining two fragments of A and B, corresponding to the organic structure (E_A) and the transition metal (E_B), respectively.

3. RESULTS AND DISCUSSION

With the aim to provide a fundamental understanding of the kinetics and thermodynamics of PDCA complexes with transition-metal ions, as illustrated in Figure 1a, we synthesize simple linear polymer precursors upon the condensation of Cl-PDCA and $PEGNH_2$10k. We use a stoichiometric ratio between the amine and acyl chloride building blocks, as even small deviations in stoichiometry limit the chain length of the resulting polymer in the condensation polymerization. However, the gel permeation chromatography (GPC) of the polymer obtained shows a weight average molar mass of 62 kg mol^{-1} and a polydispersity index of 1.9. One-week dialysis against water using a metal-free membrane with a 10 kg mol^{-1} pore size does not significantly help to obtain a narrower molar mass distribution (MMD), as shown in Figure S3. The final MMD curve demonstrates multiple shoulders, which can be assigned to PEG monomers, trimers, hexamers, and decamers, as demonstrated in Figure S4, by the deconvolution of the obtained curve into a weighted summation of four Gaussian distribution functions. Consequently, the polymer obtained contains 73% of long chains with more than two PDCA ligands, profiting from enough interchain connectivity upon complexation with metal ions to form a percolated transient polymer network. Assuming that trimers also contain at least three PDCA units, the fraction of chains that effectively contribute to network formation can increase to 92%. Nevertheless, a minor fraction of shorter chains, which is between 8 and 27%, including PEG monomers and a part of trimers, form dangling ends and chain extensions, respectively. These fractions do not effectively contribute to the network percolation and energy storage upon deformation. We form transient networks at a polymer concentration of φ = 10 v/w %, which is significantly above the overlap concentration of the polymer precursor.[60] Considering an entanglement molar mass (M_e) of 2 kg mol^{-1} for PEG at the molten state,[60,61] the effective M_e at this concentration is roughly 20 kg mol^{-1}, which shows that some loose entanglements between long chains may also contribute to the network formation. On the one hand, employing a too long $PEGNH_2$ precursor could reduce the reaction efficiency and the number of ligands along chains, which could avoid network buildup upon the formation of metal−ligand associations. On the other hand, too short precursors may result in short extended chains that despite having a larger number of ligands along them, they may not form a percolated network at the very low concentrations that are normally used for hydrogel formation. The 10 kg mol^{-1} $PEGNH_2$ precursor has a compromised length in between, so that a percolated network can be formed at the 10% w/v concentration, as discussed throughout this paper. Of course,

https://doi.org/10.1021/acs.chemmater.2c01346
Chem. Mater. 2022, 34, 6155−6169

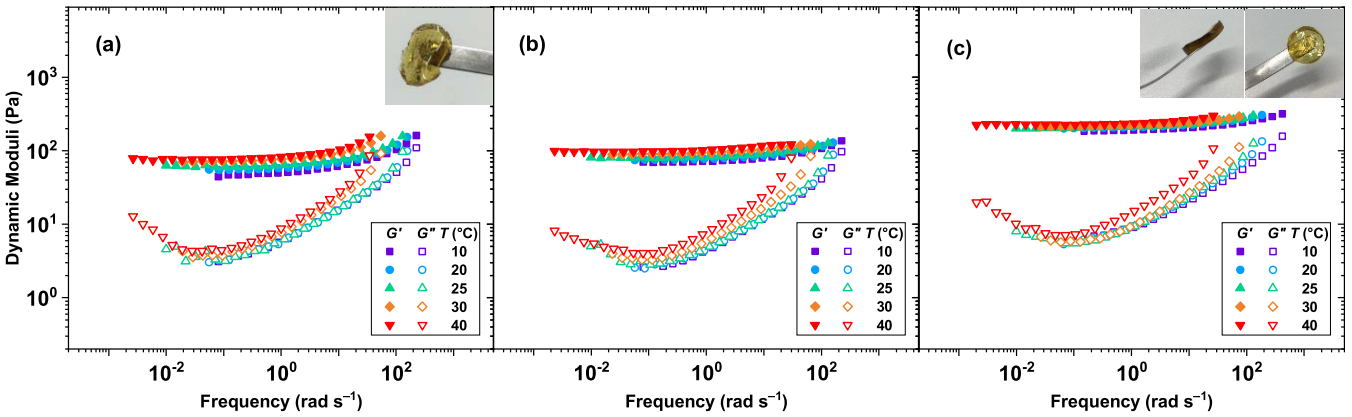

Figure 2. Dynamic storage (filled symbols) and loss (open symbols) moduli master curves (T_{ref} = 25 °C) of the networks formed at φ = 10 v/w % and PDCA/Co^{2+} = 2:1 at different sodium hydroxide concentrations: (a) OH/PDCA = 5, (b) OH/PDCA = 15, and (c) OH/PDCA = 30.

using shorter precursors would have probably required using larger polymer fractions.

PDCA is reported to form bis-complexes with Fe^{3+} and Zn^{2+}, like tridentate ligands, through sextuple coordination bonds.[39] Interestingly, these six coordination bonds are reported to have different stabilities, four of them with lateral nitrogen or oxygen atoms being labile and two of them with the central nitrogen atoms being strong, as illustrated in Figure 1b. Progressive deprotonation at larger pH values is reported to form the more stable, but entropically unfavored, complexation by both lateral amide groups. The lateral bonds can readily break and reform, while the central ones keep metal ions in the vicinity. This combination of bond dynamics specifically results in rapid self-healing. To explore the utility of this mechanism, we use nitrate salts of various transition-metal ions including Zn^{2+}, Co^{2+}, Fe^{3+}, Ni^{2+}, and Cu^{2+}, which are expected to cover a wide range of coordination stability.[43,62] Specifically, the lifetime of complexes these metal ions make with different protic and aprotic ligands is mainly reported to follow Zn^{2+} < Co^{2+} < Fe^{3+} < Ni^{2+} < Cu^{2+}, which is in accordance with the Irving−Williams series.[33,43,62−64]

The complexation of protic ligands and metal ions is reported to occur under basic conditions upon deprotonation of their heteroatoms.[32] However, transition-metal ions are expected to form hydroxide salts and precipitate in severe basic conditions. Therefore, following Holten−Andersen's method for the complexation of transition-metal ions with catechol,[65] which has also been proved to work for histidine,[66] we first mix the aqueous solution of the polymer precursor and metal ions and then increase the pH after 1 h using a 1 M solution of sodium hydroxide. The gel formation occurs locally and homogenizes over time. After 24 h, homogeneous gels are formed as shown in the inset images of Figure 2. The dynamic mechanical properties of these physical networks are mainly dominated by the thermodynamic strength and kinetic stability of reversible metallo-supramolecular bonds, which determine the number and lifetime of transient cross-links. Consequently, we study the rheological behavior of hydrogels under small-amplitude oscillatory shear (SAOS) deformation and follow the storage and loss moduli at different temperatures. The plateau modulus and the frequency at which the storage and loss moduli cross each other are directly determined by the equilibrium number and lifetime of transient cross-links, respectively.[34,35,62] As such, SAOS can provide a rich insight into the strength and stability of PDCA complexes. The slightly entangled solution of the polymer precursor does not demonstrate a viscosity noticeably larger than that of water.[67] Also, the viscosity does not change significantly upon the addition of metal ions in the absence of hydroxide ions (OH) and at high pH values without metal ions. However, progressively stronger gels form by the establishment of metallo-supramolecular complex upon increasing the pH value.

In sharp contrast to former reports, which depend heavily on the strong coordination of Fe^{3+} and PDCA in bulk,[3,37,39,41] we were unable to make a hydrogel with Fe^{3+} ions at any pH value. This might be due to the formation of monocomplexes or labile bis-complexes at neutral pH values and progressive precipitation of iron hydroxide at high pH values due to the larger affinity of iron ions to the OH ligand. Also, the formation of FeO and Fe_2O_3 or Fe_3O_4 at high pH is possible.[68] This has been probably avoided in previous studies on PDCA due to the absence of the solvent. Likewise, against former reports on the efficiency of Zn^{2+} in creating even stronger gels in bulk compared to that of Fe^{3+},[37] we could not make a gel at any pH value, neither with Zn^{2+} nor with Cu^{2+}, which is probably correlated to the lability of their bis-complexes if they form. Nevertheless, physical hydrogels are formed using Co^{2+} and Ni^{2+}, whose strength can be tuned by the ratio of OH/PDCA and PDCA/M^{2+}. Accordingly, for metals that have a high tendency to form metal oxide, it is not possible to have complexes at high pH values. Therefore, it is also possible to have ZnO and CuO precipitates at high pH values. In contrast, Co^{2+} and Ni^{2+} prefer to form highly coordinated complexes.[32]

Transient gels formed in the presence of Co^{2+} demonstrate a flat plateau modulus in all of the accessible frequency ranges, as shown in Figure 2. However, unlike chemically cross-linked gels, there are two modes of relaxation beyond the accessible high- and low-frequency limits, as understood by the corresponding upturns in the loss modulus. These modes, respectively, demonstrate the fast relaxation of dangling ends and loops in short times and the dissociation of supramolecular bonds in much longer times. The dissociation of transient bonds is reflected in the rheology spectrum only if it results in the loss of energy, which occurs only if complexes exchange their ligands.[69] Therefore, the relaxation time extracted from rheological measurements is expected to be larger than the lifetime of the complex since dissociated groups may go back to former partners several times before finding other free groups to associate with. The time−temperature superposition (tTS) does not work perfectly as the overlay at the low-

https://doi.org/10.1021/acs.chemmater.2c01346
Chem. Mater. 2022, 34, 6155−6169

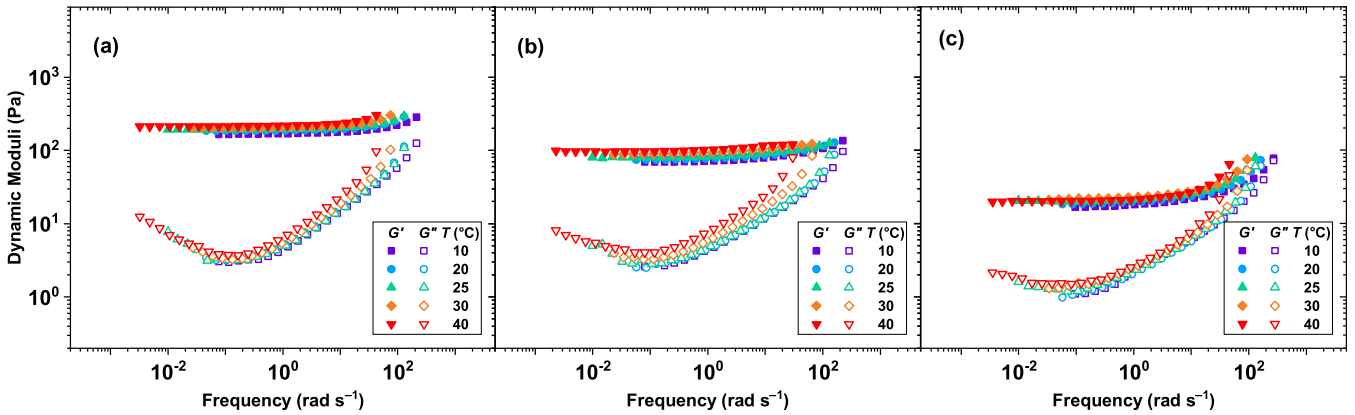

Figure 3. Dynamic storage (filled symbols) and loss (open symbols) moduli master curves (T_{ref} = 25 °C) of the networks formed at φ = 10 v/w % and OH/PDCA = 15:1 at different metal ion concentrations: (a) PDCA/Co^{2+} = 1, (b) PDCA/Co^{2+} = 2, and (c) PDCA/Co^{2+} = 4.

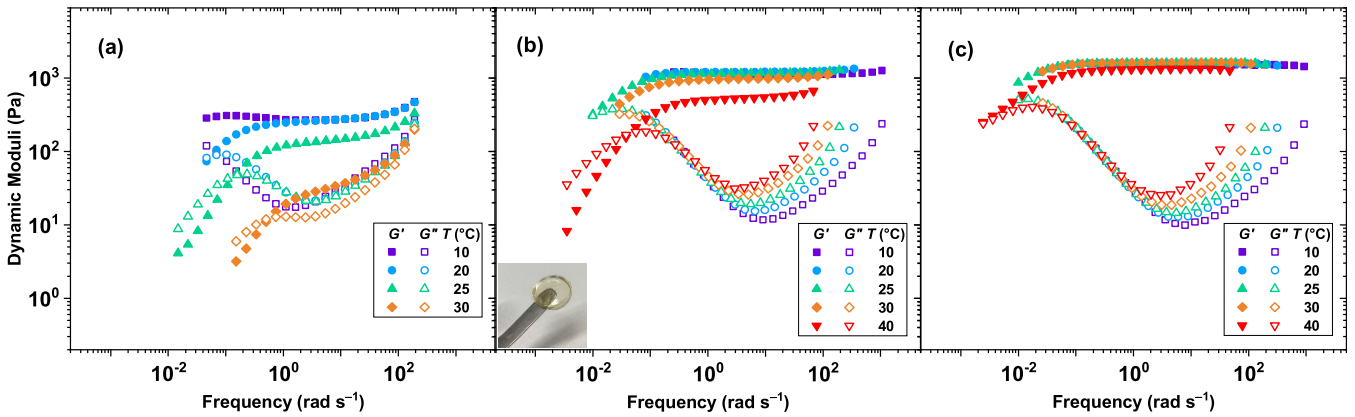

Figure 4. Dynamic storage (filled symbols) and loss (open symbols) moduli master curves (T_{ref} = 25 °C) of the networks formed at φ = 10 v/w % and PDCA/Ni^{2+} = 2:1 at different sodium hydroxide concentrations: (a) OH/PDCA = 5, (b) OH/PDCA = 15, and (c) OH/PDCA = 30. tTS is not applied to panel (a) and to the measurement at 40 °C in panel (b).

frequency limits comes with the expense of a minor mismatch at the high-frequency range. This is expected, specifically when the activation energy of the polymeric dynamics and supramolecular complexation differ significantly.[70] The plateau modulus increases monotonically as the ratio of OH/PDCA increases. This is explained by the increased concentration of deprotonated PDCA ligands, which shifts the equilibrium toward bis-complexes. The effect of the OH content on the stability of the complex, however, cannot be judged since the low-frequency crossover of the storage and loss moduli is below the accessible frequency range.

To provide a more quantitative understanding of the gelation in these samples, we confront the obtained plateau modulus with the prediction of the phantom network model

$$G_N^0 = \left(\frac{f-2}{2}\right)\mu k_B T$$

where f is the cross-link's functionality, μ is the number of network cross-links per volume, and k_BT is the thermal energy. Given the cross-link's functionality of 4, and assuming an infinite molar mass for all polymer chains, which is equivalent to neglecting all misconnectivities in the system, one can consider only bis-complexes, which results in one effective cross-link per metal ion or per two PDCA ligands at their stoichiometric concentration. As such, neglecting the minor trapped entanglements, the largest possible plateau modulus, according to the concentration of metal ions, would be 12.4 kPa. Nonetheless, the experimentally measured plateau modulus is just 70 Pa at OH/PDCA = 5, which increases to 240 Pa at OH/PDCA = 30. This difference factor of 50 not only demonstrates the significant role of misconnectivities in supramolecular polymer systems based on short linear precursors but also highlights the fact that not all current PDCA ligands and Co^{2+} ions are engaged in the formation of bis-complexes.[42,71] As such, we expect a low equilibrium constant, K, despite the very large dissociation rate constant, k_d, for the complex formed by Co^{2+}. To provide a rough estimate of the dissociation time, we fit the dynamic moduli curves obtained at 25 °C by considering two relaxation modes, each represented by a log−normal distribution of relaxation times at the high- and low-frequency ranges, as explained in the Supporting Information.[34] Interestingly, the dynamic moduli could not be reproduced unless considering two very broad relaxation modes, which results in an apparent crossover at significantly low frequencies below 10^{-5} rad s^{-1}, as shown in Figure S5a. This slow and broad relaxation can also be related to the contribution of the hindered polymeric relaxation of long chains in the presence of reversible supramolecular dynamics.[72−74] The dissociation of stable supramolecular bonds can be better understood by an exponential drop of shear stress in the stress relaxation experiment.[35,62] However, the corresponding shear stress curves only reflect a gradual power-law decay, as shown in Figure S6. This essentially limits the formation of a unique master curve by applying tTS and

https://doi.org/10.1021/acs.chemmater.2c01346
Chem. Mater. 2022, 34, 6155−6169

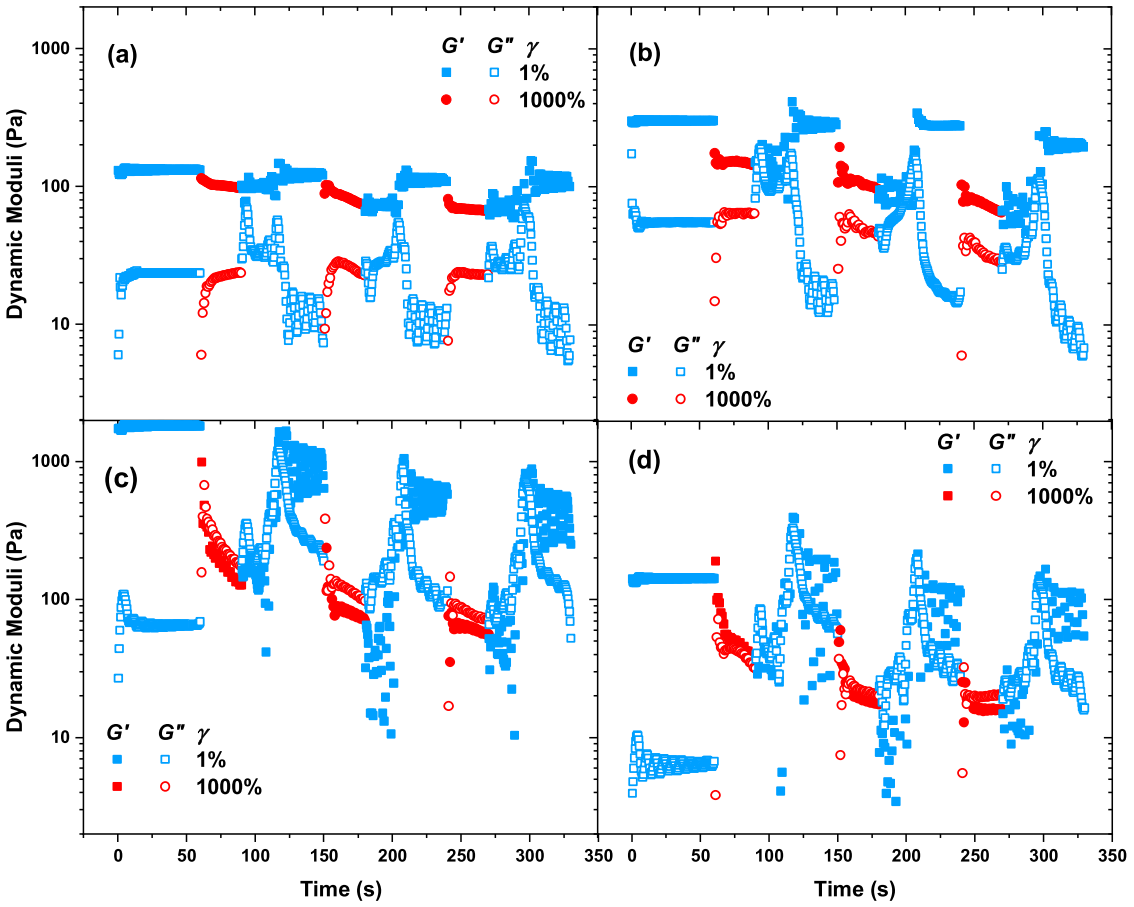

Figure 5. Dynamic storage and loss moduli at sequentially small- and large-amplitude (γ = 1 and 1000%) time-sweep measurements ($\dot{\gamma}$ = 1 rad s^{-1}) for networks formed by Co^{2+} at (a) OH/PDCA = 15 and (b) OH/PDCA = 30, and for networks formed by Ni^{2+} at (c) OH/PDCA = 15 and (d) OH/PDCA = 30, all using φ = 10 v/w % and PDCA/M^{2+} = 2:1.

further suggests the remarkable stability of bis-PDCA−Co^{2+} complexes and the broadness of the relaxation mode at low frequencies.

The low equilibrium constant associated with the Co^{2+} complex also suggests that the equilibrium can be effectively shifted toward complexation by increasing the metal ion concentration above the stoichiometry. The dynamic moduli obtained at different PDCA/Co^{2+} ratios indeed demonstrate that the plateau modulus increases upon using overstoichiometric Co^{2+} concentrations, as shown in Figure 3. Similar results are obtained by the stress relaxation measurements, as shown in Figure S7.

Metallo-supramolecular polymer networks formed by Ni^{2+} and various protic and aprotic ligands usually demonstrate greater stability compared to those made by Co^{2+}.[34,62,63,75] In contrast to this expectation, transient gels formed by the coordination of PDCA and Ni^{2+} exhibit faster relaxations compared to those made by Co^{2+}. This is demonstrated by the crossover of the dynamic moduli in the accessible frequency range, as shown in Figure 4. Following the above trend, the plateau modulus increases at higher OH/PDCA ratios. However, SOAS measurements at the highest temperature demonstrate a lower plateau modulus and a shorter relaxation time, which can be associated with the loss of network percolation upon losing a fraction of active cross-links at that temperature. The effect of temperature on network percolation is more evident at the lowest OH content, as shown in Figure 4a, which is at the margin of percolation, and may lose integrity by a simple increase in the temperature or decrease in the metal ion concentration. Consequently, tTS is not applied to this sample.

The fitted dynamic moduli, which are obtained by considering two relaxation modes at high and low frequencies, reflect a much narrower relaxation mode around 0.01 rad s^{-1}, compared to the broad one obtained for the Co^{2+}, as demonstrated in Figure S5b. The larger plateau modulus and the narrower relaxation mode suggest a larger equilibrium constant for the bis-PDCA−Ni^{2+} complex, which results in the formation of less misconnectivity and dangling ends. A similar relaxation mode with the pronounced exponential decay of shear stress is reflected in the stress relaxation curves of the corresponding samples, as demonstrated in Figure S8.

Another interesting question is whether the oxidation state of the metal ion affects the coordination characteristics. To account for that, we follow Wegner's approach and oxidize Co^{2+} using a stoichiometric amount of hydrogen peroxide overnight.[75] Subsequently, the Co^{3+} is mixed with the precursor solution and then the pH is increased. The obtained dynamic moduli demonstrate even a larger plateau modulus compared to that obtained with Co^{2+} at the same OH content, as demonstrated in Figure S9. Histidine has also been reported to form stronger bonds with significantly greater stabilities after the oxidation of Co^{2+} to Co^{3+}.[75,76]

One of the prime utilities of metallo-supramolecular polymer networks is in self-healing applications. The characteristic time of self-healing and its efficiency are expected to scale directly

https://doi.org/10.1021/acs.chemmater.2c01346
Chem. Mater. 2022, 34, 6155−6169

with the stability and inversely with the strength of transient bonds, respectively.[77−79] Therefore, the change in the metal ion and pH value should have notable effects on the self-healing characteristics of PDCA-extended polymers. To check this notion, we employ sequential large- and small-amplitude time-sweep measurements to, respectively, destruct the network structure and monitor its reconstruction. We utilize short deconstruction segments of 30 s and reconstruction segments of 60 s to challenge the healing rate of the networks. The obtained storage moduli reveal that the networks formed by Co^{2+} demonstrate fast deconstruction followed by rapid and near-complete recovery, as shown in Figure 5a,b. Despite the destruction amplitude increases at larger OH concentrations, the degree of recovery remains near-complete. In contrast, networks formed by Ni^{2+} demonstrate larger deconstruction amplitude so that the network percolation is lost, as comprehended from loss moduli exceeding the storage moduli, followed by gradual and incomplete network buildup, as shown in Figure 5c,d. This is in contrast to the expectation based on the shorter lifetime of bis-PDCA−Ni^{2+} complexes compared to those made by Co^{2+}.[80] Nevertheless, another important prerequisite for self-healing is the presence of free ligands to immediately reform deconstructed complexes.[77] Regarding its lower thermodynamic equilibrium constant, such free PDCA ligands are expected to be more available in networks formed by Co^{2+} rather than those formed by Ni^{2+}. A similar fast deconstruction followed by rapid and near-complete recovery is obtained for the networks formed by Co^{3+}, as shown in Figure S10. This further highlights the importance of the presence of free ligands or using thermodynamically less strong complexes for self-healing applications.

Our rheological studies demonstrate unexpected results on the association of different transition-metal ions with PDCA. The flow activation energies obtained from tTS for hydrogels formed by either Co^{2+} and Ni^{2+} increase at larger OH contents, as demonstrated in the upper panel of Figure 6. The largest E_a values obtained for Co^{2+} and Ni^{2+} are 67 and 73 kJ mol^{-1}, which are in the same range as those obtained for aprotic ligands such as terpyridine and phenanthroline.[43,62] This is clear evidence for the pH tunability of complexation and gel formation. Nevertheless, this tunability also depends on the coordination affinity of the utilized metal ion, as suggested by distinct developments of the plateau modulus upon increasing the OH/PDCA ratio, as shown in the middle panel of Figure 6. The deprotonation of the ligand is an important step for achieving larger coordination numbers. To confirm this hypothesis, potentiometry measurements are performed by titrating a dilute aqueous solution of the precursor (10 mg in 5 mL) in the presence of NaCl (10 mM) with a NaOH solution (1 N) and monitoring the pH value. The obtained pH curve demonstrates the lack of sequential deprotonation steps and implies that the majority of coordinating atoms should be already available at OH/PDCA ratios as low as 5, as demonstrated in the lower panel of Figure 6. This is in sharp contrast with the gradual increase of the network's mechanical properties at higher OH/PDCA ratios. Therefore, the correlation between the coordination geometry and deprotonation level of the ligand remains a prime open question. Moreover, it is also surprising that among the metal ions studied, only Co^{2+} and Ni^{2+} are able to form a gel, whereas Fe^{3+} and Zn^{2+} cannot. We seek to answer these questions through spectroscopic and theoretical DFT studies.

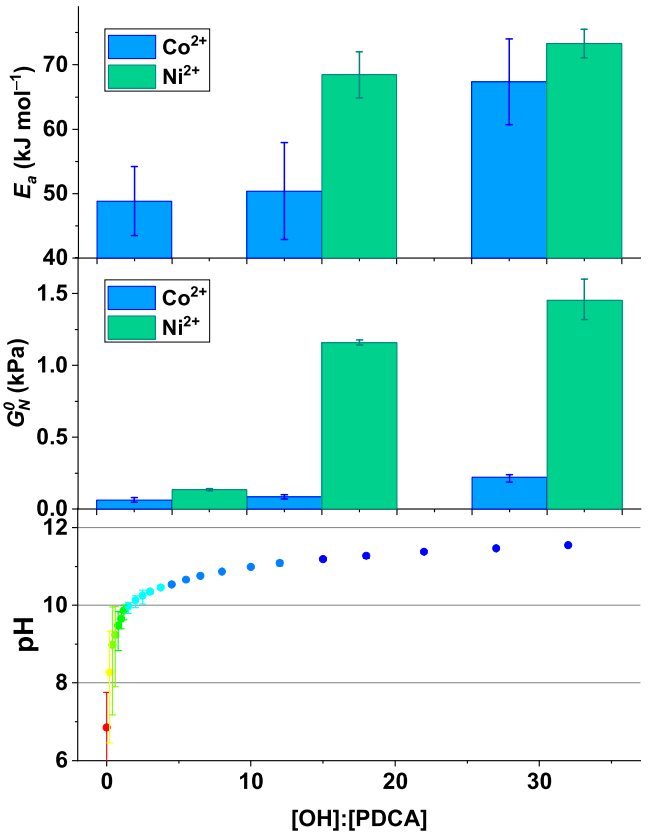

Figure 6. Flow activation energies of the networks formed by Co^{2+} and Ni^{2+} at φ = 10 v/w % and PDCA/M^{2+} = 2:1 at different OH/PDCA ratios (upper panel), the corresponding plateau moduli measured at a frequency of 1 rad s^{-1} (middle panel), and the measured pH values at different OH/PDCA ratios (lower panel).

To further examine the complexation of different metal ions with PDCA, we follow the absorption spectra of a dilute aqueous solution of the polymer precursor in the presence of stoichiometric amounts of metal ions at various OH contents. For this purpose, we prepare the aqueous solution of the polymer precursor and metal ion; after 1 h, we increase the pH, and after 24 h, we measure the UV−Vis spectra. The evolution of the characteristic complex absorption bands at different metal ion concentrations could be used to determine the equilibrium constant. Also, the time-dependent decay of the absorption intensity upon adding a second metal ion with a stronger association constant could be employed to calculate the dissociation rate constant.[81] Nevertheless, none of the complexes show a significant change in the absorption spectra after increasing the pH, as demonstrated in Figure 7a. This can also be inferred from the pale colors of the corresponding gels shown in the inset images of Figures 2 and 4. The polymer solution obtained using Fe^{3+} has a dark orange color, which is reflected by several distinct absorptions in the visible and UV ranges. However, the lack of network formation confirms the lability of such bonds or the prevalence of mono-PDCA−Fe^{3+} complexes. As such, UV−Vis studies could not significantly help in studying the kinetics and thermodynamics of PDCA complexes.

The structure of complexes is further characterized by the Fourier transform infrared (FTIR) spectroscopy. Several bands show distinct variations among samples even in the aqueous solution, as shown in Figure S11. However, the spectra in the

https://doi.org/10.1021/acs.chemmater.2c01346
Chem. Mater. 2022, 34, 6155−6169

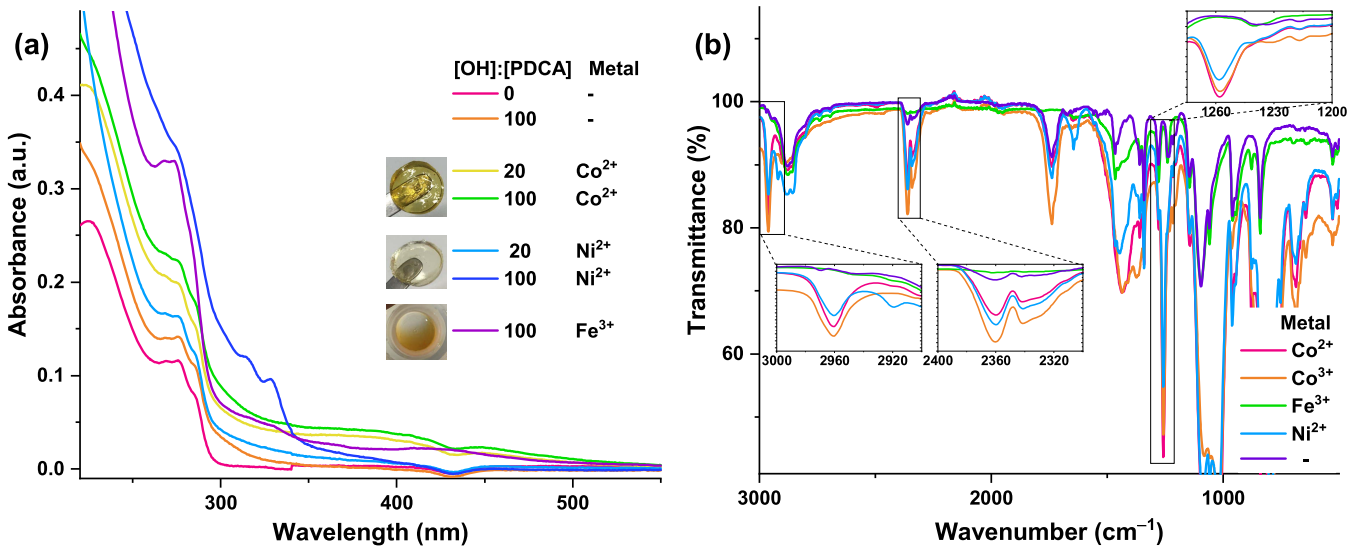

Figure 7. (a) UV−Vis spectra of the plain polymer precursor and stoichiometric mixtures with different metal ions at various OH/PDCA contents. (b) FTIR spectra of the plain polymer precursor and stoichiometric mixtures with different metal ions at OH/PDCA = 100 in the dry state.

Table 1. Relative Energies (in kcal mol^{-1}) of Bis-PDCA Complexes (CO, Coordination through the Carbonyl; N, Coordination through the Nitrogen) with Respect to the Nondeprotonated Systems[a]

Mode of coordination	Protonation level	Co^{2+}	Co^{3+}	Fe^{2+}	Fe^{3+}	Ni^{2+}	Ni^{3+}	Zn^{2+}
0CO-2N	-2 protons	-27.4[a]	-32.5	-5.0	-33.4	-45.7	-33.3	-19.3
1CO-1N	-2 protons	-33.7[a]	-60.6	-32.1	-62.8	-44.2	-56.3	-21.4
2CO-0N	-2 protons	-19.3	-42.6	-18.3	-43.3	-30.0	-42.5	-19.7
0CO-2N	-1 proton	9.9	9.0	24.2	10.6	-14.1	-9.8	-8.8
1CO-1N	-1 proton	-5.2	-20.5	-2.7	-21.0	-27.8	-23.5	-13.5
2CO-0N	-1 proton	-13.7	-23.1	-7.9	-23.4	-17.9	-26.0	-4.8
0CO-2N	No deprotonation	-	57.3	-	66.9	-	55.6	25.9
1CO-1N	No deprotonation	24.0	27.9	-	29.4	9.8	31.0	6.1
2CO-0N	No deprotonation	0.0	0.0	0.0[a]	0.0	0.0	0.0	0.0

[a]The high spin species are denoted in blue; -not possible coordination with the metal.

solution are highly affected by the absorption of the solvent. Therefore, we perform the same measurement on identical samples after drying. Similar trends are observed between spectra in dried samples; *i.e.*, complexes formed in the presence of Co^{2+}, Co^{3+}, and Ni^{2+} show similar distinct absorption peaks, whereas the plain polymer precursor and its mixture with Fe^{3+} follow a very similar trend, as shown in Figure 7b. This specifically includes the N−H stretch bands below 3000 cm^{-1}, as highlighted in the inset plot of Figure 7b, and the amide C═O bands around 1700 cm^{-1}, as highlighted in the inset plot of Figure S11, which are significantly amplified upon complexation with Co^{2+}, Co^{3+}, and Ni^{2+}.

To provide an understanding of the relationship between the microscopic characteristics of the constructing units and macroscopic material functions, specifically the pH dependence of the rheological behavior and the underlying reason for different performances of the utilized metal ions, we study the coordination geometry of the equivalent small-molecule complexes. To accelerate calculations, we replace the terminal polymer chains from both sides of the PDCA ligand with a methyl group. Given the possible coordination modes between the ligand and metal ions in Figure 1, we envisage DFT calculations. The study is applied to the oxidation states of +2 and +3 for Co, Fe, and Ni, as described in Table 1, with additional calculations also for Zn^{2+}. Accordingly, the tests of the pristine ligand suggest that the deprotonation of both amide groups is not favored in the absence of any metal ions,[82,83] with a cost of 7.1 kcal mol^{-1} compared to the single deprotonation that is nearly isoenergetic with the pristine ligand, *i.e.*, just being 0.1 kcal mol^{-1} higher in energy. Afterward, the deprotonation in the presence of metal ions is studied. We consider all possible protonation levels of the PDCA ligand by the stepwise removal of all four protons of lateral amide groups, as listed in Table 1, for a selected number of samples. The coordination mode is coded as *X*CO−*Y*N, where *X* and *Y* denote the number of coordinated lateral oxygen and nitrogen atoms participating in the formation of bis-complexes from each ligand, respectively, besides the coordinated central pyridyl nitrogen atom. DFT results suggest that the most stable mode of coordination is the octahedral geometry. According to Table 1 results, the symmetric geometry is favored; *i.e.*, each ligand of the metal complex loses one proton. Structurally, the coordination of the pyridyl group is always present, and the two remaining coordinating groups may be the carbonyl or the amino groups. However, at the employed pH levels, one of the amino groups from each

https://doi.org/10.1021/acs.chemmater.2c01346
Chem. Mater. 2022, 34, 6155−6169

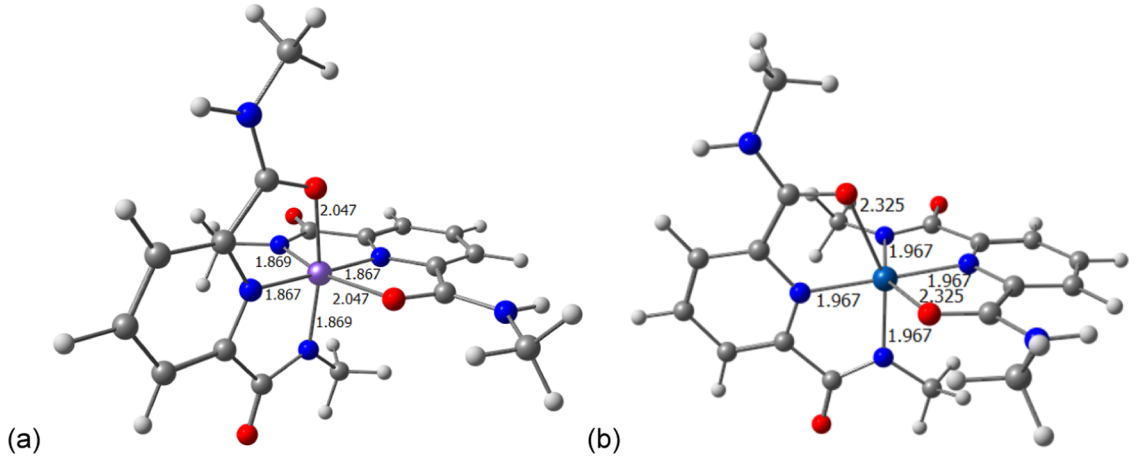

Figure 8. Best coordination for (a) Fe^{3+} and (b) Co^{2+} with two anionic PDCA ligands (selected distances given in Å).

Table 2. Binding Energies (in kcal mol^{-1}) of Two Ligands on Each Metal Center[a]

Protonation level	Co^{2+}	Co^{3+}	Fe^{2+}	Fe^{3+}	Ni^{2+}	Ni^{3+}	Zn^{2+}
-2 protons	-56.4[a]	-89.2[a]	-32.7	-37.8	-60.1	-74.6	-28.9
-1 proton	-36.4	-51.8	-8.6	1.6	-42.1	-44.2	-21.1
No deprotonation	-22.7	-28.7	-0.6[a]	25.0	-14.4	-18.2	-7.6

[a]The high spin species are denoted in blue.

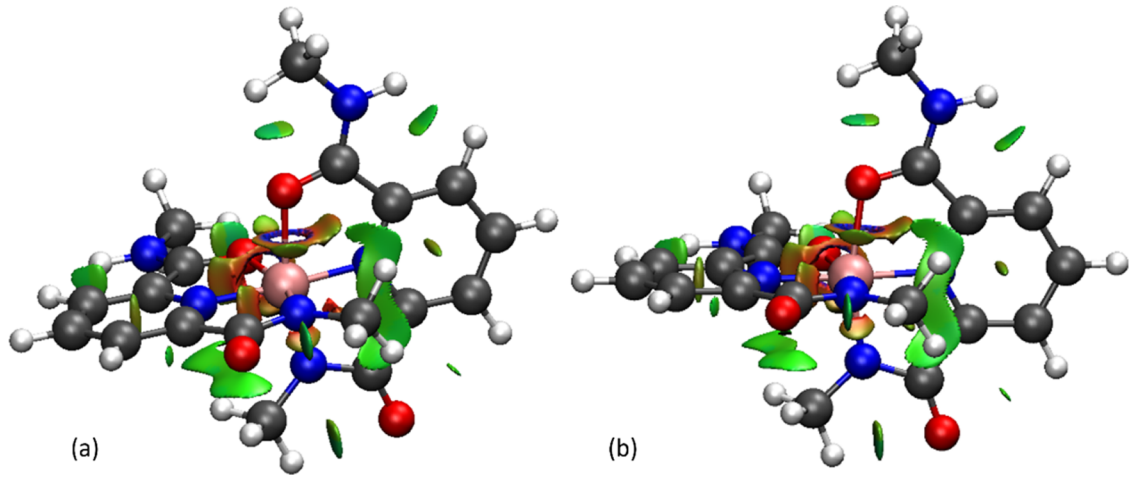

Figure 9. NCI plots for (a) the systems with Co^{3+} and (b) with Fe^{3+} (green and blue isosurfaces depict weak- and strong-attractive interactions, respectively, while red isosurface represents strong-repulsive interactions).

tridentate ligand easily deprotonates. This favors the coordination of the metal ion with the deprotonated amino and the carbonyl group of each ligand, as shown in Figure 8. However, for the special case of Ni^{2+}, the coordination through the carbonyl is never favored but only by a 1.5 kcal mol^{-1} cost of energy. Therefore, the excessive deprotonation at larger pH values and the formation of the entropically unfavored complex upon the association of lateral amide groups, as suggested in Figure 1b, are not a general case and, in contrast with former reports, may rarely occur.

The binding energy of the employed metal ions with the PDCA ligand suggests that the interaction is clearly stronger for cobalt and then at a very close margin for nickel; however, iron shows the poorest values by far, as listed in Table 2. This is a confirmation that when adding the metal ion solution, together at the basic pH, the preference is the loss of one proton from each ligand, thus two protons for each metal center. All of these results fit with experiments, particularly, when no gelation was observed with the iron and zinc ions. In detail, comparing the neutral and anionic ligands, cobalt is the best metal bearing the neutral ligand, whereas, for two anionic ligands, Ni^{2+} could even enhance its binding compared to cobalt. In any case, iron or zinc would be less competitive. Structurally, the comparison of the interaction strength of metal ions with both ligands,[84] by means of the Mayer bond orders (MBOs),[85,86] shows the lability of the coordinative bonds formed by Ni^{2+}, Ni^{3+}, and Zn^{2+} ions, with a clear decrease.[87,88] Actually, the sum of the MBO values for the six M−O and M−N interactions is 2.687, 2.470, and 2.343, respectively, which are at least 1 unit lower than that for the cobalt-based systems (see Table S1 for further details).[89]

https://doi.org/10.1021/acs.chemmater.2c01346
Chem. Mater. 2022, 34, 6155−6169

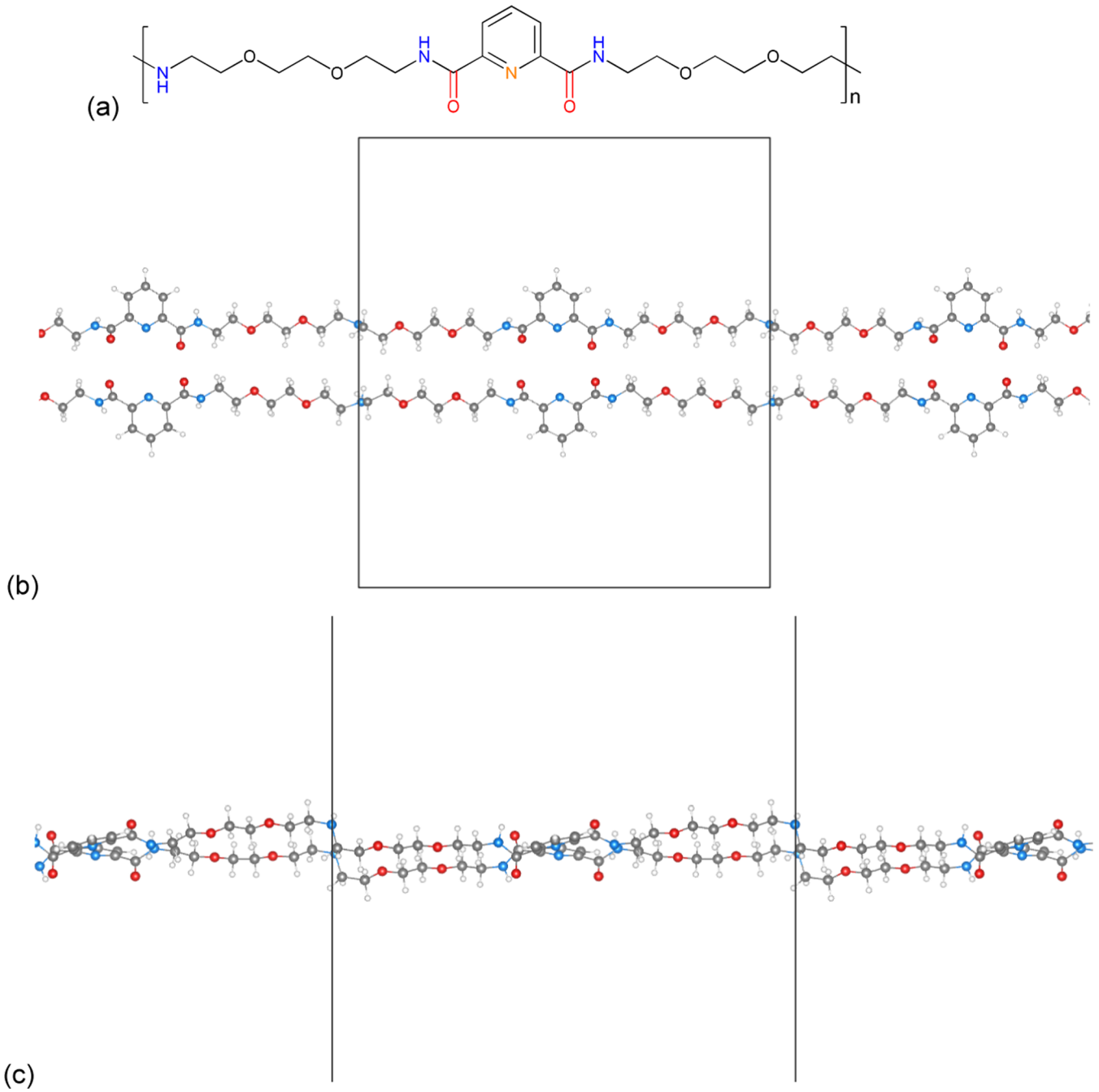

Figure 10. (a) Repeating unit selected to perform the calculations under PBC. (b) Representation of the optimized organic periodic structure showing the periodicity on the *Y* axis (the repeating unit within the optimized cubic cell inside the square is also represented), front view. (c) Same structure, top view.

Notably, the M^{3+} ion should be preferred over the M^{2+} ones according to the explained results. To further study the effect of the oxidation state, we removed one of the ligands from the complexes formed by the single deprotonated PDCAs, and the destabilization follows as Ni^{3+} (74.2) > Co^{3+} (65.5) > Fe^{3+} (54.8) > Ni^{2+} (38.2) > Fe^{2+} (37.6) > Co^{2+} (35.2) kcal mol^{-1}. Thus, clearly, M^{3+} species need two ligands. Moreover, the addition of chloride atoms to compensate the positive charge on the monometal complexes confirms the same trend: Fe^{3+} (55.2 (37.1)) > Co^{3+} (57.3 (36.8)) > Fe^{2+} (35.5) > Co^{2+} (24.7) > Ni^{3+} (35.2(19.5)) > Ni^{2+} (11.1) kcal mol^{-1}. In parentheses, the values with two chlorides instead of one to complete the whole positive charge of systems bearing M^{3+} ion metals are reported.

The noncovalent interaction (NCI) plots reveal the importance of the aryl ring of both ligands. Figure 9 demonstrates how both ligands for complexes formed with Co^{3+} and Fe^{3+} are stabilized by those relatively weak interactions. A relatively strong interaction between the aryl ring and the methylenic moiety in the α position to the nitrogen of amides is present. According to the NCI plots, the interaction is strong since it has a tridentate capacity to bind to the metal ions (see the Supporting Information for further details). However, the more stabilizing interaction of Co^{3+} is not that clear compared to the less efficient complexation of

https://doi.org/10.1021/acs.chemmater.2c01346
Chem. Mater. 2022, 34, 6155−6169

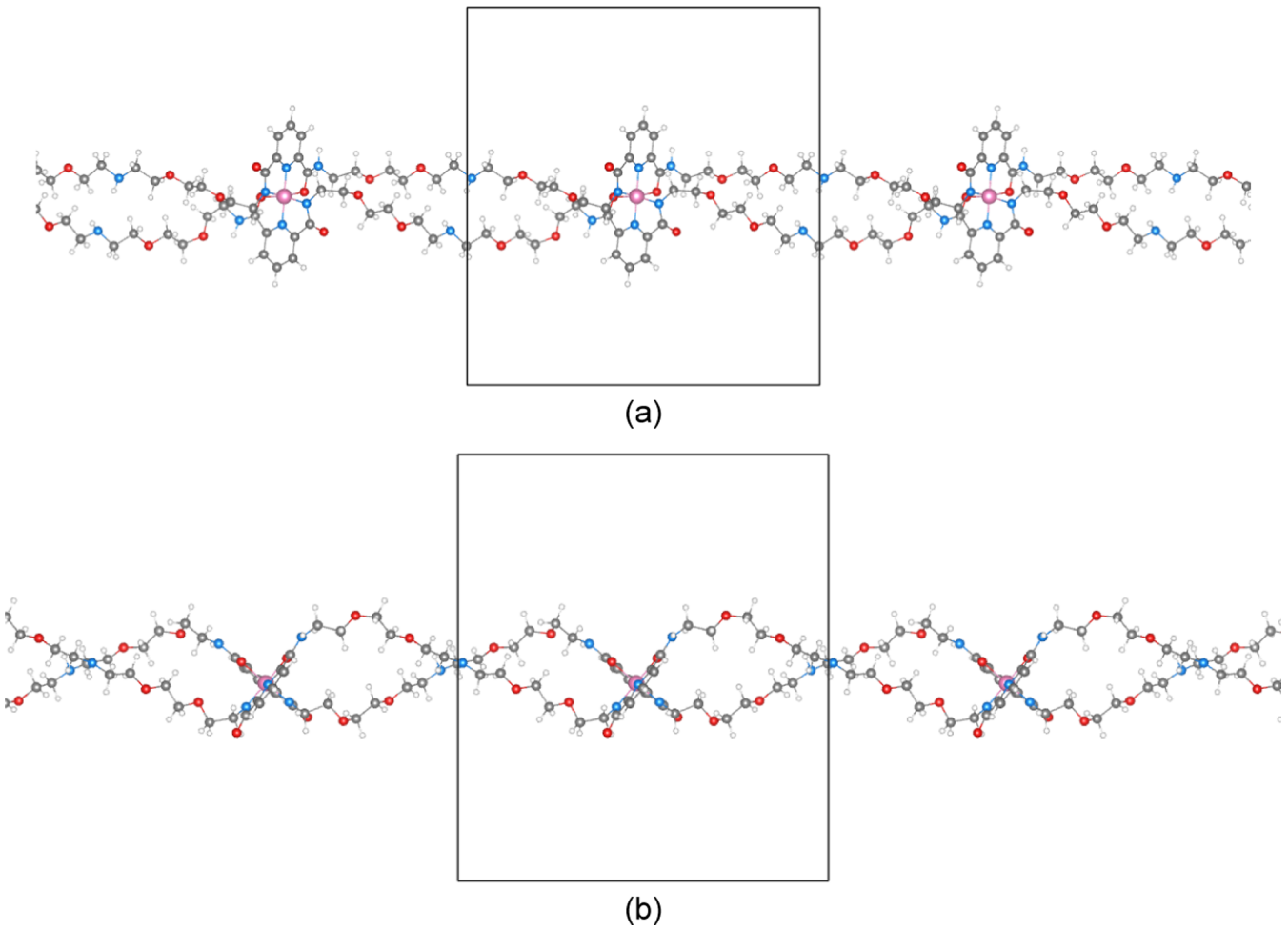

Figure 11. (a) Front view and (b) top view of the optimized structure for the [Co^{2+}] complex.

Fe^{3+}. When comparing both NCI plots in detail, only a few differences imply the slightly more stabilizing interactions for Co^{3+}, which are not clear enough in Figure 9.

To provide further details on the UV−Vis spectroscopy results that are presented in Figure 7, we employ TD-DFT calculations (see Table S2). Despite the spectral complexity, the bands that show the most significant differences upon complexation are in the region below 300 nm. Therefore, these calculations confirm that the deprotonation of the two ligands coordinated to metal ions is not accompanied by a significant variation of absorptions in the region between 300 and 400 nm. This is in agreement with experiments, where no change of absorption is detected upon complexation with different metal ions, except for the Ni^{2+}, which also reflects bands between 300 and 320 nm in computational results.

The observed noncovalent interactions in the simplified systems represented in Figure 9 are not comprehensive enough to compare the nature of metal ions. As such, due to the incapacity of static DFT calculations to provide a clear trend among the complexation of different metal ions, we employ periodic DFT calculations by means of CP2K. To deal with the presence of PEG precursors along with PDCA ligands coordinated with transition-metal ions, the system is expanded compared to the simple static DFT calculations by Gaussian. Specifically, as shown in Figure 1a, the repeating unit of this polymer includes a 10 kg mol^{-1} PEG segment coupled with a PDCA ligand. However, to obtain a proper description of the organic chains as well as the coordination of metal ions, which is yet computationally affordable, a simplified structure based on a short PEG linker is considered, as shown in Figure 10a (geometry containing 118 atoms). At first, cell optimization of only the periodic organic part is performed to obtain the cell parameters and confirm the periodicity of the system. The structure is first included at the center of a cubic box of 25 × 25 × 25 $Å^3$, ensuring isolation on the *X* and *Z* axes, and only the periodicity on the *Y* axis is considered (the geometry of this polymer has a length of approximately 27 Å), as shown in Figure 10b,c (see Tables S3 and S4). The optimization of the organic part confirms that the structure has been properly constructed, consistently reproducing the periodicity of the system only on the *Y* axis. The optimized cell parameters have been used to construct the cell for the next calculations to study the systems after the incorporation of the desired transition-metal ions.

The above description of the structural optimization without including the metal center is really interesting. Since once repeated in the presence of metal ions, and after performing the cell optimization (including both cell parameter optimization and geometry relaxation), a dramatic modification of the conformation of the polymeric system emerges. After the complexation of the PDCA ligands with the metal center, they adopt an important torsion in their structures and form a helicoidal structure, as shown in Figure 11a,b. For the system with Fe^{3+}, the metal center is coordinated with two

https://doi.org/10.1021/acs.chemmater.2c01346
Chem. Mater. 2022, 34, 6155−6169

deprotonated N atoms as well as two O atoms, forcing each PDCA ligand to turn, which leads to the torsion of the entire organic tail. Accordingly, the same helicoidal-like structure is confirmed for all of the different metal ions under study.

Energetically, the binding energy calculations considering BSSE corrections and posteriorly addition of the solvent corrections considering water and dichloromethane as the solvents lead to data collected in Table 3, suggesting that, both

Table 3. Binding Energies (in kcal mol^{-1}) in Gas Phase, Water, and Dichloromethane between the Two Organic Chains and the Metal Center

	binding energies		
system	gas phase	water	dichloromethane
Co^{2+}	−187.05	−75.02	−66.08
Co^{3+}	−140.06	−49.19	−39.66
Fe^{2+}	−242.28	−136.11	−126.77
Fe^{3+}	−136.92	−39.20	−28.27
Ni^{2+}	−161.84	−74.16	−65.05
Ni^{3+}	−90.31	−11.79	−5.06

in gas phase and in the presence of the solvent, systems with M^{2+} present higher binding energies than those where M^{3+} metal centers are engaged. This could seem a paradox since the latter metal centers should be more electrophilic and bond more strongly to organic ligands. However, in agreement with experimental results, systems with Co^{2+} and Ni^{2+} show the largest coordination affinity (excluding the system with Fe^{2+}, which shows the largest binding energy in calculations, but it was not evaluated experimentally due to the probable oxidation to Fe^{3+}), followed by Co^{3+} and Fe^{3+}, remaining finally Ni^{3+} with the lowest binding energy. Consequently, periodic DFT also explains the gel formation of systems with stronger binding energies. Binding energies in the gas phase are all relatively high; however, when considering solvation, those values are dramatically reduced. Therefore, periodic DFT also implies the crucial role of solvent. In contrast to former experimental reports, which were mainly obtained in bulk, we were unable to form hydrogels with the Fe^{3+} metal ion. When considering the solvation effects, the binding energy between the metal center and the ligand is substantially reduced. As such, in Fe^{3+} systems, the formation of the hydrogel through the complexation of PDCA enters in competition with other side reactions, like the formation of iron oxide or iron hydroxide precipitates that have stronger interactions than complexation.

Reperforming the analysis of the noncovalent interactions, the NCI plots of the periodic systems considering periodicity in the *Y* axis become relevant to better understand not only the metal−ligand interactions but also the noncovalent interactions between organic PEG segments. In detail, initially it was thought that the interaction between the two organic tails would be irrelevant, especially compared to the complexes formed through the metal center. However, interestingly, they adopt a helicoidal-like structure. It is easy to compare those systems with the most known helicoidal structure, the DNA. Indeed, this results in an overstabilization of the network structure. Even, the main characteristics such as mechanical strength and self-healing could also stem from this structure and the interaction between PEG segments. For instance, Figure 12 includes the representative NCI plots for systems with Co^{2+} and Fe^{3+}, with a clear emphasis on the relevant

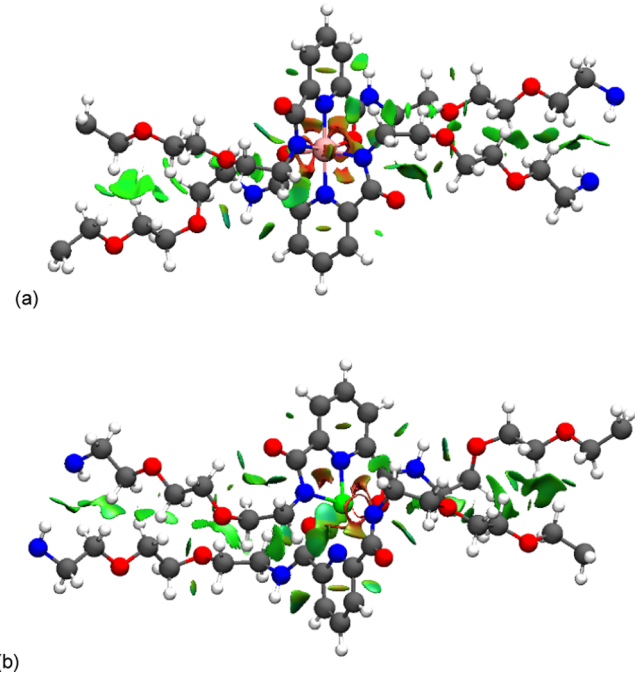

Figure 12. NCI plots for the systems containing (a) Co^{2+} and (b) Ni^{2+} (green and blue isosurfaces depict weak- and strong-attractive interactions, respectively, while red isosurface represent strong-repulsive interactions).

number of weak interactions between the two tails, offering an overstabilization of the system that would not be possible, or at least significantly reduced, with the linearity of the two tails.

4. CONCLUSIONS

This work provides a fundamental understanding of the kinetics and thermodynamics of PDCA complexes with a series of transition-metal ions. This acquired knowledge can be used as a basis for expanding the application of this ligand in the development of metallo-supramolecular polymer hydrogels and networks. To achieve that, we condensate linear PEG segments with the PDCA ligand through urethane linkages and form hydrogels by the complexation of PDCA with various metal ions at basic conditions. The rheological studies reveal the progressive formation of transient bonds upon increasing pH using $Co^{2+/3+}$ and Ni^{2+} but not with Fe^{3+}, Zn^{2+}, and Cu^{2+}. Static DFT simulations indeed confirm that interactions are clearly stronger for Co and Ni, and Fe shows the poorest values by far. Energetically, the strength of binding energies marks the difference between ions in gel formation due to the competitivity with side complexations. This competition is increased in the presence of the solvent, as metal centers such as iron can easily form salts and precipitate without forming the desired hydrogel. The system under study includes PEG segments extended with the PDCA ligand that is complexed with transition-metal ions; as a result, we can envision a unidirectional periodic structure based on two chains. The analyses of NCI plots allowed us to qualitatively unveil the importance of the noncovalent interactions between not only the metal−ligand complexes but also PEG segments. Specifically, chains rearrange themselves after the coordination, leading to a helicoidal-like structure that offers extra stability and as such promotes material properties. A perfect network with all active strands and associated transient bonds has the

https://doi.org/10.1021/acs.chemmater.2c01346
Chem. Mater. 2022, 34, 6155−6169

least potential for adhesion. However, in side-chain systems like our samples, with small complexation equilibrium constants, the potential for adhesion and accordingly self-healing is very high. Therefore, these hydrogels have high potentials for applications that required self-healing and adhesion.

■ ASSOCIATED CONTENT

Supporting Information

The Supporting Information is available free of charge at https://pubs.acs.org/doi/10.1021/acs.chemmater.2c01346.

Additional SEC, ^{1}H NMR, FTIR, UV−Vis, and stress relaxation data; description of the extended Maxwell model; tabulated UV−Vis spectra predicted by TD-DFT; xyz coordinates of the optimized structures; CP2K cell parameters; and NCI plots (PDF)

■ AUTHOR INFORMATION

Corresponding Authors

Mostafa Ahmadi − *Department of Chemistry, Johannes Gutenberg University Mainz, 55128 Mainz, Germany;* orcid.org/0000-0001-6652-4067; Email: ahmadi@uni-mainz.de

Albert Poater − *Institut de Química Computacional i Catàlisi, Departament de Química, Universitat de Girona, 17003 Girona, Catalonia, Spain;* orcid.org/0000-0002-8997-2599; Email: albert.poater@udg.edu

Authors

Farhad Panahi − *Institut für Organische Chemie, Albert-Ludwigs-Universität Freiburg, 79104 Freiburg im Breisgau, Germany;* orcid.org/0000-0003-0420-4409

Naeimeh Bahri-Laleh − *Polymerization Engineering Department, Iran Polymer and Petrochemical Institute (IPPI), Tehran 14977 13115, Iran;* orcid.org/0000-0002-0925-5363

Mohammad Sabzi − *Department of Mechanical Engineering, North Dakota State University, Fargo, North Dakota 58102, United States;* orcid.org/0000-0003-3891-9429

Gerard Pareras − *School of Chemistry, University College Cork, T12 YN60 Cork, Ireland; Institut de Química Computacional i Catàlisi, Departament de Química, Universitat de Girona, 17003 Girona, Catalonia, Spain*

Bruno N. Falcone − *School of Chemistry, University College Cork, T12 YN60 Cork, Ireland; Institut de Química Computacional i Catàlisi, Departament de Química, Universitat de Girona, 17003 Girona, Catalonia, Spain;* orcid.org/0000-0003-0114-9213

Complete contact information is available at: https://pubs.acs.org/10.1021/acs.chemmater.2c01346

Notes

The authors declare no competing financial interest.

■ ACKNOWLEDGMENTS

M.A. would like to thank the German Research Foundation (DFG) for their financial support via the independent research grant number 491930291. A.P. is a Serra Húnter Fellow and ICREA Academia Prize 2019. A.P. thanks the Ministerio de Economía y Competitividad (MINECO) for project PGC2018-097722-B-I00. N.B.-L. thanks Iran Polymer and Petrochemical Institute for its support through fund No. 43794115. G.P. and B.N.F. gratefully acknowledge the support of the Institut de Química Computacional i Catàlisi (IQCC) and the computer resources and technical support provided by the Barcelona Supercomputing Center (BSC).

■ REFERENCES

(1) Liu, X.; Liu, J.; Lin, S.; Zhao, X. Hydrogel machines. *Mater. Today* **2020**, *36*, 102−124.

(2) Talebian, S.; Mehrali, M.; Taebnia, N.; Pennisi, C. P.; Kadumudi, F. B.; Foroughi, J.; Hasany, M.; Nikkhah, M.; Akbari, M.; Orive, G.; Dolatshahi-Pirouz, A. Self-healing hydrogels: the next paradigm shift in tissue engineering? *Adv. Sci.* **2019**, *6*, No. 1801664.

(3) Jia, Z.-R.; Zeng, Y.; Tang, P.-F.; Gan, D.-L.; Xing, W.-S.; Hou, Y.; Wang, K.-F.; Xie, C.-M.; Lu, X. Conductive, Tough, Transparent, and Self-Healing Hydrogels Based on Catechol-Metal Ion Dual Self-Catalysis. *Chem. Mater.* **2019**, *31*, 5625−5632.

(4) Hou, S.; Ma, P. X. Stimuli-Responsive Supramolecular Hydrogels with High Extensibility and Fast Self-Healing via Precoordinated Mussel-Inspired Chemistry. *Chem. Mater.* **2015**, *27*, 7627−7635.

(5) Li, C. H.; Zuo, J. L. Self-healing polymers based on coordination bonds. *Adv. Mater.* **2019**, *32*, No. 1903762.

(6) Herbst, F.; Döhler, D.; Michael, P.; Binder, W. H. Self-healing polymers via supramolecular forces. *Macromol. Rapid Commun.* **2013**, *34*, 203−220.

(7) Khare, E.; Holten-Andersen, N.; Buehler, M. J. Transition-metal coordinate bonds for bioinspired macromolecules with tunable mechanical properties. *Nat. Rev. Mater.* **2021**, *6*, 421−436.

(8) Yuan, J.; Fang, X.; Zhang, L.; Hong, G.; Lin, Y.; Zheng, Q.; Xu, Y.; Ruan, Y.; Weng, W.; Xia, H.; Chen, G. Multi-responsive self-healing metallo-supramolecular gels based on "click" ligand. *J. Mater. Chem.* **2012**, *22*, 11515−11522.

(9) Samai, S.; Biradha, K. Chemical and Mechano Responsive Metal-Organic Gels of Bis(benzimidazole)-Based Ligands with Cd(II) and Cu(II) Halide Salts: Self Sustainability and Gas and Dye Sorptions. *Chem. Mater.* **2012**, *24*, 1165−1173.

(10) Bera, S.; Chakraborty, A.; Karak, S.; Halder, A.; Chatterjee, S.; Saha, S.; Banerjee, R. Multistimuli-Responsive Interconvertible Low-Molecular Weight Metallohydrogels and the in Situ Entrapment of CdS Quantum Dots Therein. *Chem. Mater.* **2018**, *30*, 4755−4761.

(11) Karimi, S.; Bahri-Laleh, N.; Sadjadi, S.; Pareras, G.; Nekoomanesh-Haghighi, M.; Poater, A. Pd on nitrogen rich polymer-halloysite nanocomposite as an environmentally benign and sustainable catalyst for hydrogenation of polyalfaolefin based lubricants. *J. Ind. Eng. Chem.* **2021**, *97*, 441−451.

(12) Das, T. K.; Poater, A. Review on Use of Heavy Metal Deposits from Water Treatment Waste towards Catalytic Chemical Syntheses. *Int. J. Mol. Sci.* **2021**, *22*, 13383.

(13) Degtyar, E.; Harrington, M. J.; Politi, Y.; Fratzl, P. The mechanical role of metal ions in biogenic protein-based materials. *Angew. Chem., Int. Ed.* **2014**, *53*, 12026−12044.

(14) Gong, J. P. Why are double network hydrogels so tough? *Soft Matter* **2010**, *6*, 2583−2590.

(15) Lehn, J. M. Perspectives in chemistry—steps towards complex matter. *Angew. Chem., Int. Ed.* **2013**, *52*, 2836−2850.

(16) Harrington, M. J.; Masic, A.; Holten-Andersen, N.; Waite, J. H.; Fratzl, P. Iron-clad fibers: a metal-based biological strategy for hard flexible coatings. *Science* **2010**, *328*, 216−220.

(17) Waite, J. H. Mussel adhesion−essential footwork. *J. Exp. Biol.* **2017**, *220*, 517−530.

(18) Ahn, B. K. Perspectives on mussel-inspired wet adhesion. *J. Am. Chem. Soc.* **2017**, *139*, 10166−10171.

(19) Mozhdehi, D.; Ayala, S.; Cromwell, O. R.; Guan, Z. Self-healing multiphase polymers via dynamic metal−ligand interactions. *J. Am. Chem. Soc.* **2014**, *136*, 16128−16131.

(20) Chen, Y.; Kushner, A. M.; Williams, G. A.; Guan, Z. Multiphase design of autonomic self-healing thermoplastic elastomers. *Nat. Chem.* **2012**, *4*, 467−472.

(21) Jangizehi, A.; Ahmadi, M.; Seiffert, S. Emergence, evidence, and effect of junction clustering in supramolecular polymer materials. *Mater. Adv.* **2021**, *2*, 1425−1453.
(22) Yu, S.; Zuo, H.; Xu, X.; Ning, N.; Yu, B.; Zhang, L.; Tian, M. Self-Healable Silicone Elastomer Based on the Synergistic Effect of the Coordination and Ionic Bonds. *ACS Appl. Polym. Mater.* **2021**, *3*, 2667−2677.
(23) Yang, H.; Ghiassinejad, S.; Van Ruymbeke, E.; Fustin, C.-A. Tunable interpenetrating polymer network hydrogels based on dynamic covalent bonds and metal−ligand bonds. *Macromolecules* **2020**, *53*, 6956−6967.
(24) Song, Y.; Liu, Y.; Qi, T.; Li, G. L. Towards Dynamic but Supertough Healable Polymers through Biomimetic Hierarchical Hydrogen-Bonding Interactions. *Angew. Chem., Int. Ed.* **2018**, *57*, 13838−13842.
(25) Sautaux, J.; Montero de Espinosa, L.; Balog, S.; Weder, C. Multistimuli, multiresponsive fully supramolecular orthogonally bound polymer networks. *Macromolecules* **2018**, *51*, 5867−5874.
(26) Brassinne, J.; Gohy, J.-F.; Fustin, C.-A. Orthogonal Control of the Dynamics of Supramolecular Gels from Heterotelechelic Associating Polymers. *ACS Macro Lett.* **2016**, *5*, 1364−1368.
(27) Meurer, J.; Baetz, T.; Hniopek, J.; Zechel, S.; Schmitt, M.; Popp, J.; Hager, M. D.; Schubert, U. S. Dual crosslinked metallopolymers using orthogonal metal complexes as rewritable shape-memory polymers. *J. Mater. Chem. A* **2021**, *9*, 15051−15058.
(28) Meurer, J.; Hniopek, J.; Bätz, T.; Zechel, S.; Enke, M.; Vitz, J.; Schmitt, M.; Popp, J.; Hager, M. D.; Schubert, U. S. Shape-Memory Metallopolymers Based on Two Orthogonal Metal−Ligand Interactions. *Adv. Mater.* **2021**, *33*, No. 2006655.
(29) Götz, S.; Zechel, S.; Hager, M. D.; Newkome, G. R.; Schubert, U. S. Versatile Applications of Metallopolymers. *Prog. Polym. Sci.* **2021**, *119*, No. 101428.
(30) Dzhardimalieva, G. I.; Yadav, B. C.; Singh, S.; Uflyand, I. E. Self-healing and shape memory metallopolymers: state-of-the-art and future perspectives. *Dalton Trans.* **2020**, *49*, 3042−3087.
(31) Koziol, M. F.; Fischer, K.; Seiffert, S. Structural and Gelation Characteristics of Metallo-Supramolecular Polymer Model-Network Hydrogels Probed by Static and Dynamic Light Scattering. *Macromolecules* **2021**, *54*, 4375−4386.
(32) Hosseinzadeh, B.; Ahmadi, M.*Coordination Geometry in Metallo-Supramolecular Polymer Networks*, Available at DOI: 10.2139/ssrn.4005928, 2022.
(33) Grindy, S. C.; Learsch, R.; Mozhdehi, D.; Cheng, J.; Barrett, D. G.; Guan, Z.; Messersmith, P. B.; Holten-Andersen, N. Control of hierarchical polymer mechanics with bioinspired metal-coordination dynamics. *Nat. Mater.* **2015**, *14*, 1210−1216.
(34) Ahmadi, M.; Seiffert, S. Thermodynamic control over energy dissipation modes in dual-network hydrogels based on metal−ligand coordination. *Soft Matter* **2020**, *16*, 2332−2341.
(35) Ahmadi, M.; Seiffert, S. Direct Evidence of Heteroleptic Complexation in the Macroscopic Dynamics of Metallo-supramolecular Polymer Networks. *Macromolecules* **2021**, *54*, 7113−7124.
(36) Mo, S.-R.; Lai, J.-C.; Zeng, K.-Y.; Wang, D.-P.; Li, C.-H.; Zuo, J.-L. New insights into the mechanical and self-healing properties of polymers cross-linked by Fe (iii)-2, 6-pyridinedicarboxamide coordination complexes. *Polym. Chem.* **2019**, *10*, 362−371.
(37) Zhang, Q.; Zhu, X.; Li, C.-H.; Cai, Y.; Jia, X.; Bao, Z. Disassociation and reformation under strain in polymer with dynamic metal−ligand coordination cross-linking. *Macromolecules* **2019**, *52*, 660−668.
(38) Liu, S.; Li, K.; Hussain, I.; Oderinde, O.; Yao, F.; Zhang, J.; Fu, G. A Conductive Self-Healing Double Network Hydrogel with Toughness and Force Sensitivity. *Chem. - Eur. J.* **2018**, *24*, 6632−6638.
(39) Li, C.-H.; Wang, C.; Keplinger, C.; Zuo, J.-L.; Jin, L.; Sun, Y.; Zheng, P.; Cao, Y.; Lissel, F.; Linder, C.; et al.*et al.* A highly stretchable autonomous self-healing elastomer. *Nat. Chem.* **2016**, *8*, 618−624.
(40) Zhang, L.; Wang, D.; Xu, L.; Zhang, A. A supramolecular polymer with ultra-stretchable, notch-insensitive, rapid self-healing and adhesive properties. *Polym. Chem.* **2021**, *12*, 660−669.
(41) Tian, M.; Zuo, H.; Wang, J.; Ning, N.; Yu, B.; Zhang, L. A silicone elastomer with optimized and tunable mechanical strength and self-healing ability based on strong and weak coordination bonds. *Polym. Chem.* **2020**, *11*, 4047−4057.
(42) Ahmadi, M.; Löser, L.; Fischer, K.; Saalwächter, K.; Seiffert, S. Connectivity Defects and Collective Assemblies in Model Metallo-Supramolecular Dual-Network Hydrogels. *Macromol. Chem. Phys.* **2020**, *221*, No. 1900400.
(43) Ahmadi, M.; Seiffert, S. Dynamic Model Metallo-Supramolecular Dual-Network Hydrogels with Independently Tunable Network Crosslinks. *J. Polym. Sci.* **2020**, *58*, 330−342.
(44) Frisch, M. J.; Trucks, G. W.; Schlegel, H. B.; Scuseria, G. E.; Robb, M. A.; Cheeseman, J. R.; Scalmani, G.; Barone, V.; Petersson, G. A.; Nakatsuji, H.; Li, X.; Caricato, M.; Marenich, A. V.; Bloino, J.; Janesko, B. G.; Gomperts, R.; Mennucci, B.; Hratchian, H. P.; Ortiz, J. V.; Izmaylov, A. F.; Sonnenberg, J. L.; Williams-Young, D.; Ding, F.; Lipparini, F.; Egidi, F.; Goings, J.; Peng, B.; Petrone, A.; Henderson, T.; Ranasinghe, D.; Zakrzewski, V. G.; Gao, J.; Rega, N.; Zheng, G.; Liang, W.; Hada, M.; Ehara, M.; Toyota, K.; Fukuda, R.; Hasegawa, J.; Ishida, M.; Nakajima, T.; Honda, Y.; Kitao, O.; Nakai, H.; Vreven, T.; Throssell, K.; Montgomery, J. A., Jr.; Peralta, J. E.; Ogliaro, F.; Bearpark, M. J.; Heyd, J. J.; Brothers, E. N.; Kudin, K. N.; Staroverov, V. N.; Keith, T. A.; Kobayashi, R.; Normand, J.; Raghavachari, K.; Rendell, A. P.; Burant, J. C.; Iyengar, S. S.; Tomasi, J.; Cossi, M.; Millam, J. M.; Klene, M.; Adamo, C.; Cammi, R.; Ochterski, J. W.; Martin, R. L.; Morokuma, K.; Farkas, O.; Foresman, J. B.; Fox, D. J. *Gaussian 16*, revision C.01; Gaussian, Inc.: Wallingford CT, 2016.
(45) Stephens, P. J.; Devlin, F. J.; Chabalowski, C. F.; Frisch, M. J. Ab initio calculation of vibrational absorption and circular dichroism spectra using density functional force fields. *J. Phys. Chem. A* **1994**, *98*, 11623−11627.
(46) Becke, A. D. Density-functional thermochemistry. III. The role of exact exchange. *J. Chem. Phys.* **1993**, *98*, 5648−5652.
(47) Lee, C.; Yang, W.; Parr, R. G. Development of the Colle-Salvetti correlation-energy formula into a functional of the electron density. *Phys. Rev. B* **1988**, *37*, 785.
(48) Weigend, F. Accurate Coulomb-fitting basis sets for H to Rn. *Phys. Chem. Chem. Phys.* **2006**, *8*, 1057−1065.
(49) Weigend, F.; Ahlrichs, R. Balanced basis sets of split valence, triple zeta valence and quadruple zeta valence quality for H to Rn: Design and assessment of accuracy. *Phys. Chem. Chem. Phys.* **2005**, *7*, 3297−3305.
(50) Leininger, T.; Nicklass, A.; Stoll, H.; Dolg, M.; Schwerdtfeger, P. The accuracy of the pseudopotential approximation. II. A comparison of various core sizes for indium pseudopotentials in calculations for spectroscopic constants of InH, InF, and InCl. *J. Chem. Phys.* **1996**, *105*, 1052−1059.
(51) Küchle, W.; Dolg, M.; Stoll, H.; Preuss, H. Energy-adjusted pseudopotentials for the actinides. Parameter sets and test calculations for thorium and thorium monoxide. *J. Chem. Phys.* **1994**, *100*, 7535−7542.
(52) Häussermann, U.; Dolg, M.; Stoll, H.; Preuss, H.; Schwerdtfeger, P.; Pitzer, R. Accuracy of energy-adjusted quasirelativistic ab initio pseudopotentials: all-electron and pseudopotential benchmark calculations for Hg, HgH and their cations. *Mol. Phys.* **1993**, *78*, 1211−1224.
(53) Falivene, L.; Barone, V.; Talarico, G. Unraveling the role of entropy in tuning unimolecular vs. bimolecular reaction rates: The case of olefin polymerization catalyzed by transition metals. *Mol. Catal.* **2018**, *452*, 138−144.
(54) Tomasini, M.; Duran, J.; Simon, S.; Azofra, L. M.; Poater, A. Towards Mild Conditions by Predictive Catalysis via Sterics in the Ru-Catalyzed Hydrogenation of Thioesters. *Mol. Catal.* **2021**, *510*, No. 111692.
(55) Coufourier, S.; Gaignard-Gaillard, Q.; Lohier, J.-F.; Poater, A.; Gaillard, S.; Renaud, J.-L. Hydrogenation of CO_2, Hydrogenocar-

bonate, and Carbonate to Formate in Water using Phosphine Free Bifunctional Iron Complexes. *ACS Catal.* **2020**, *10*, 2108−2116.
(56) Hutter, J.; Iannuzzi, M.; Schiffmann, F.; VandeVondele, J. cp2k: atomistic simulations of condensed matter systems. *Wiley Interdiscip. Rev.: Comput. Mol. Sci.* **2014**, *4*, 15−25.
(57) Perdew, J. P.; Ruzsinszky, A.; Csonka, G. I.; Vydrov, O. A.; Scuseria, G. E.; Constantin, L. A.; Zhou, X.; Burke, K. Restoring the density-gradient expansion for exchange in solids and surfaces. *Phys. Rev. Lett.* **2008**, *100*, No. 136406.
(58) VandeVondele, J.; Hutter, J. Gaussian basis sets for accurate calculations on molecular systems in gas and condensed phases. *J. Chem. Phys.* **2007**, *127*, No. 114105.
(59) Andreussi, O.; Dabo, I.; Marzari, N. Revised self-consistent continuum solvation in electronic-structure calculations. *J. Chem. Phys.* **2012**, *136*, No. 064102.
(60) Schmolke, W.; Ahmadi, M.; Seiffert, S. Enhancement of metallo-supramolecular dissociation kinetics in telechelic terpyridine-capped poly (ethylene glycol) assemblies in the semi-dilute regime. *Phys. Chem. Chem. Phys.* **2019**, *21*, 19623−19638.
(61) Cavallaro, G.; Lazzara, G.; Pignon, F.; Chiappisi, L.; Paineau, E. Effect of Polymer Length on the Adsorption onto Aluminogermanate Imogolite Nanotubes. *Langmuir* **2021**, *37*, 9858−9864.
(62) Ahmadi, M.; Seiffert, S. Coordination geometry preference regulates the structure and dynamics of metallo-supramolecular polymer networks. *Macromolecules* **2021**, *54*, 1388−1400.
(63) Grindy, S. C.; Lenz, M.; Holten-Andersen, N. Engineering elasticity and relaxation time in metal-coordinate cross-linked hydrogels. *Macromolecules* **2016**, *49*, 8306−8312.
(64) Mozhdehi, D.; Neal, J. A.; Grindy, S. C.; Cordeau, Y.; Ayala, S.; Holten-Andersen, N.; Guan, Z. Tuning dynamic mechanical response in metallopolymer networks through simultaneous control of structural and temporal properties of the networks. *Macromolecules* **2016**, *49*, 6310−6321.
(65) Holten-Andersen, N.; Harrington, M. J.; Birkedal, H.; Lee, B. P.; Messersmith, P. B.; Lee, K. Y. C.; Waite, J. H. pH-induced metal-ligand cross-links inspired by mussel yield self-healing polymer networks with near-covalent elastic moduli. *Proc. Natl. Acad. Sci. U.S.A.* **2011**, *108*, 2651−2655.
(66) Fullenkamp, D. E.; He, L.; Barrett, D. G.; Burghardt, W. R.; Messersmith, P. B. Mussel-inspired histidine-based transient network metal coordination hydrogels. *Macromolecules* **2013**, *46*, 1167−1174.
(67) Ahmadi, M.; Seiffert, S. Efficiency range of the Belousov−Zhabotinsky reaction to induce the self-organization of transient bonds in metallo-supramolecular polymeric systems. *Phys. Chem. Chem. Phys.* **2020**, *22*, 14965−14975.
(68) Kim, S.; Regitsky, A. U.; Song, J.; Ilavsky, J.; McKinley, G. H.; Holten-Andersen, N. In situ mechanical reinforcement of polymer hydrogels via metal-coordinated crosslink mineralization. *Nat. Commun.* **2021**, *12*, No. 667.
(69) Rubinstein, M.; Semenov, A. N. Dynamics of entangled solutions of associating polymers. *Macromolecules* **2001**, *34*, 1058−1068.
(70) Zhang, Z.; Huang, C.; Weiss, R.; Chen, Q. Association energy in strongly associative polymers. *J. Rheol.* **2017**, *61*, 1199−1207.
(71) Nicolella, P.; Koziol, M. F.; Löser, L.; Saalwächter, K.; Ahmadi, M.; Seiffert, S. Defect-controlled softness, diffusive permeability, and mesh-topology of metallo-supramolecular hydrogels. *Soft Matter* **2022**, *18*, 1071−1081.
(72) Ahmadi, M.; Hawke, L. G.; Goldansaz, H. Van Ruymbeke, E. Dynamics of entangled linear supramolecular chains with sticky side groups: Influence of hindered fluctuations. *Macromolecules* **2015**, *48*, 7300−7310.
(73) Hawke, L. G. D.; Ahmadi, M.; Goldansaz, H.; Van Ruymbeke, E. Viscoelastic properties of linear associating poly (n-butyl acrylate) chains. *J. Rheol.* **2016**, *60*, 297−310.
(74) Ahmadi, M.; Jangizehi, A.; van Ruymbeke, E.; Seiffert, S. Deconvolution of the Effects of Binary Associations and Collective Assemblies on the Rheological Properties of Entangled Side-Chain Supramolecular Polymer Networks. *Macromolecules* **2019**, *52*, 5255−5267.
(75) Wegner, S. V.; Schenk, F. C.; Witzel, S.; Bialas, F.; Spatz, J. P. Cobalt cross-linked redox-responsive PEG hydrogels: From viscoelastic liquids to elastic solids. *Macromolecules* **2016**, *49*, 4229−4235.
(76) Li, P.; Xia, Y.; Hao, J.; Wang, X. Transient healability of metallosupramolecular polymer networks mediated by kinetic control of competing chemical reactions. *Macromolecules* **2020**, *53*, 2856−2863.
(77) Appel, E. A.; Forster, R. A.; Koutsioubas, A.; Toprakcioglu, C.; Scherman, O. A. Activation Energies Control the Macroscopic Properties of Physically Cross-Linked Materials. *Angew. Chem., Int. Ed.* **2014**, *53*, 10038−10043.
(78) Cordier, P.; Tournilhac, F.; Soulié-Ziakovic, C.; Leibler, L. Self-healing and thermoreversible rubber from supramolecular assembly. *Nature* **2008**, *451*, 977−980.
(79) Xiao, Z.-Y.; Zhao, X.; Jiang, X.-K.; Li, Z.-T. Tunable Coordinative Assembly of a Disc-Like Molecule and Metal Ions: From Mirospheres to Microtubes and Microrods. *Chem. Mater.* **2011**, *23*, 1505−1511.
(80) Xu, X.; Jerca, V. V.; Hoogenboom, R. Self-Healing Metallo-Supramolecular Hydrogel Based on Specific Ni^{2+} Coordination Interactions of Poly (ethylene glycol) with Bistriazole Pyridine Ligands in the Main Chain. *Macromol. Rapid Commun.* **2020**, *41*, No. 1900457.
(81) Thordarson, P. Determining association constants from titration experiments in supramolecular chemistry. *Chem. Soc. Rev.* **2011**, *40*, 1305−1323.
(82) Luque-Urrutia, J. A.; Solà, M.; Poater, A. The Influence of the pH on the Reaction Mechanism of Water Oxidation by a Ru (bda) Catalyst. *Catal. Today* **2020**, *358*, 278−283.
(83) Luque-Urrutia, J. A.; Kamdar, J. M.; Grotjahn, D. B.; Solà, M.; Poater, A. Understanding the performance of a bisphosphonate Ru water oxidation catalyst. *Dalton Trans.* **2020**, *49*, 14052−1406.
(84) Kaur, S.; Kumar, V.; Chawla, M.; Cavallo, L.; Poater, A.; Upadhyay, N. Pesticides curbing soil fertility: effect of complexation of free metal ions. *Front. Chem.* **2017**, *5*, No. 43.
(85) Mayer, I. Charge, bond order and valence in the AB initio SCF theory. *Chem. Phys. Lett.* **1983**, *97*, 270−274.
(86) Poater, A.; Gallegos Saliner, A.; Solà, M.; Cavallo, L.; Worth, A. P. Computational Methods to Predict the Reactivity of Nanoparticles Through Structure-Property Relationships. *Expert Opin. Drug Delivery* **2010**, *7*, 295−305.
(87) Poater, A.; Gimferrer, G.; Poater, A. Covalent and Ionic Capacity of MOFs To Sorb Small Gas Molecules. *Inorg. Chem.* **2018**, *57*, 6981−6990.
(88) Tabrizi, M.; Sadjadi, S.; Pareras, G.; Nekoomanesh-Haghighi, M.; Bahri-Laleh, N.; Poater, A. Efficient hydro-finishing of polyalfaolefin based lubricants under mild reaction condition using Pd on ligands decorated halloysite. *J. Colloid Interface Sci.* **2021**, *581*, 939−953.
(89) Luque-Urrutia, J. A.; Solà, M.; Milstein, D.; Poater, A. Mechanism of the Manganese-Pincer Catalyzed Acceptorless Dehydrogenative Coupling of Nitriles and Alcohols. *J. Am. Chem. Soc.* **2019**, *141*, 2398−2403.

https://doi.org/10.1021/acs.chemmater.2c01346
Chem. Mater. 2022, 34, 6155−6169